Anisotropic Fluorescence Emission and Photobleaching of Fluorophores in Proximity of One Dimensional Photonic Crystals sustaining Bloch Surface Waves. II. Experiments

ELISABETTA SEPE[1], ALBERTO SINIBALDI[1], NORBERT DANZ[2], PETER MUNZERT[2], AND FRANCESCO MICHELOTTI[1,*]

[1] *Department of Basic and Applied Science for Engineering, Sapienza University of Rome, Via A. Scarpa 16, 00161 Rome, Italy*
[2] *Fraunhofer Institute for Applied Optics and Precision Engineering, A.-Einstein-Str. 7, 07745 Jena, Germany*
** francesco.michelotti@uniroma1.it*

ABSTRACT

Photonic crystal (PC) enhanced fluorescence has been proposed as a novel tool for early disease detection in liquid biopsy. Photobleaching of the emitters has never been deeply investigated, despite its cross section is expected to increase due to the large field intensity enhancement in PC. Herein, we report on the experimental investigation of the anisotropic effects arising when fluorescence excitation and emission are coupled to differently polarized modes of the same PC structure. In particular, we experimentally characterized the anisotropic photobleaching taking place during the operation of one dimensional PC (1DPC) biosensors sustaining Bloch surface waves (BSW) at their truncation edge. The experimental results are compared to the description provided by our theoretical model reported in a twin article. We demonstrate experimentally that photobleaching affects the response of a cancer biomarkers' detection assay and propose a procedure to compensate for it. Moreover, we describe the experimental use of BSW coupled fluorescence and of the strong localization of the BSW at the 1DPC surface to selectively probe the rotational diffusion kinetics of proteins bound at the 1DPC surface with high spatial resolution and for different binding strengths.

1. INTRODUCTION

Recently, in a theoretical article, we addressed the modeling of photobleaching (PB) of fluorescent dye molecules bound at the surface of one dimensional photonic crystals (1DPC) [1]. In particular, we analyzed the consequences arising from the action of anisotropic PB on the reliability of fluorescence based 1DPC biosensors and the possibility to exploit it to probe the orientation of the emitters. We evidenced that PB cannot be neglected in biosensing applications, especially when targeting analytes concentrations are very close to their limit of detection [2], in relation to the relevant literature [3].

Here, we report on experiments aimed at characterizing anisotropic PB in real fluorescence biosensing assays carried out with 1DPC biochips. In particular we used 1DPC fluorescence biosensors sustaining Bloch surface waves (BSW) at their truncation interface [4–6]. Similarly to the surface plasmon polariton (SPP) case [3], fluorescence emitters in proximity of the surface of the 1DPC can couple to the BSW, leading to enhanced excitation rates and BSW-coupled emission [7], therefore providing opportunities for new fluorescence sensing schemes [8].

In literature on photonic crystal (PC) biosensors, despite the large intensity enhancement factors reported, PB was either not cited or only offhandedly discussed, except some isolated cases in which it was investigated experimentally during the operation of PC biosensors [9], without however addressing the anisotropic effects [3] arising when the fluorescence excitation and emission are coupled to differently polarized modes of the same PC structure. Also for 1DPC biosensors, PB was never deeply discussed [6,10]. Usually, in both PC and 1DPC enhanced stationary fluorescence biosensors, the orientational distribution of emitters is assumed to be isotropic, even if the excitation is polarized [7,8,11], based on the assumption that fluorescence depolarization always dominates [3,12]. However, for emitters bound at a surface, as for most of PC or 1DPC fluorescence biosensors, such an assumption could be wrong since rotational motion might be hindered.

On the other hand, since BSW can be either TE or TM polarized [4], contrarily to SPP, a significant portion of the emission of a fluorescently labelled protein in proximity of a 1DPC can couple to the available BSW, either TE or TM [13], owing to the large local density of optical states (LDOS) provided by the 1DPC [11]. Detecting the relative intensities of the TE and TM BSW components can therefore permit to trace back to the emitters/proteins' orientation and eventually to their kinetics under non equilibrium conditions [1]. It is therefore of particular interest to perform time resolved BSW fluorescence emission experiments.

The prospect of observing conformational changes of proteins by detecting changes in the dipole orientation of a rigidly attached probe [14] is among the most exciting possibilities opened up by room-temperature fluorescence polarization anisotropy techniques, in their ensemble [3,15] and single molecule versions [16–19]. It is of particular interest to characterize rotational motion of biomolecules which are either immobilized at a surface [20,21] or embedded in a membrane / layer. [15,22]

Here, we report on the experimental use of BSW coupled fluorescence and of the strong localization of the BSW at the 1DPC surface to selectively probe rotational diffusion only of those proteins that are bound at the 1DPC surface. The experimental results should be compared to the results provided by our theoretical model. [1]

2. FABRICATION OF THE 1DPC BIOCHIPS

The 1DCP biochips used in the present work were designed to sustain BSW in the visible range when operating in water environment [1]. The design was transferred to real devices by depositing the 1DPC onto optical quality organic substrates with a prism shaped cross section that permits to operate in the attenuated total internal reflection (TIR) configuration (Kretschmann-Raether) [23], as shown in Figure 1a-b. The substrates were obtained by replica molding [24] a cyclic olefin copolymer (TOPAS 5013 LS) [25]. Additionally, a two-component flow cell was molded (Figure 1a), consisting of a hard polymer cover that can be clicked onto the chip. Inside this cover an elastomer defines three straight micro channels (0.8 x 0.1 mm^2 cross section) as well as perpendicularly aligned fluid connectors. In the present work we used only the middle micro channel.

The 1DPC were deposited onto the substrates by plasma ion assisted electron beam evaporation (PIAD) of inorganic dielectric layers under high vacuum conditions (3×10^{-4} mbar, Leybold Optics APS904 coating system) [26]. Since PIAD permits to coat at low substrate temperature (< 100 °C), it is suitable for the 1DPC deposition on plastics. After cleaning, the substrates were preconditioned by plasma etching at low ion energies for 60 s. The 1DPC was then obtained by evaporating tantalum oxide (Ta_2O_5), silicon dioxide (SiO_2) and titanium dioxide (TiO_2). In order to achieve low internal stress and absorption losses in the layers, a medium level argon ion assistance with ion energies of about 80 eV was applied.

The geometry of the 1DPC is shown in Figure 1c and is based on two pairs of bilayers, each constituted by a Ta_2O_5 and a SiO_2 high and low refractive index layers with the thicknesses of d_H = 120 nm and d_L = 275 nm, respectively. An additional SiO_2 layer with thickness d_L was first deposited onto the substrate to improve the reliability of the stack. The 1DPC was topped with a TiO_2 / SiO_2 bilayer, with thickness of both layers d_T = 20 nm. A quartz crystal oscillator was used for thickness monitoring during the deposition.

The PIAD deposition technique allows for a precision better than 1.5% for the thick layers and better than 1.5 nm for the thin layers [26]. In Figure 1c we also show a FESEM image of the cross section of a 1DPC deposited on a reference cover slip substrate after coating with a thin graphite layer (~10nm). Within the resolution provided by the FESEM under the conditions achievable with an insulating sample, the thicknesses of the layers match the design values.

The complex refractive indices at λ_{LF} = 670 nm of Ta_2O_5, SiO_2 and TiO_2 are $\tilde{n}_H = 2.160 + j5 \times 10^{-5}$, $\tilde{n}_L = 1.474 + j5 \times 10^{-6}$ and $\tilde{n}_T = 2.28 + j1.8 \times 10^{-3}$, respectively. They were measured by reflectance/transmittance spectroscopy of single layers deposited on reference substrates. The extinction coefficients were too small to be determined by spectrophotometry and were obtained by measuring the BSW reflectivity of reference 1DPC in a broad angular range [27]. The substrate and water / solution refractive indices at λ_{LF} are n_{sub} = 1.526 and n_{sol} = 1.328, respectively.

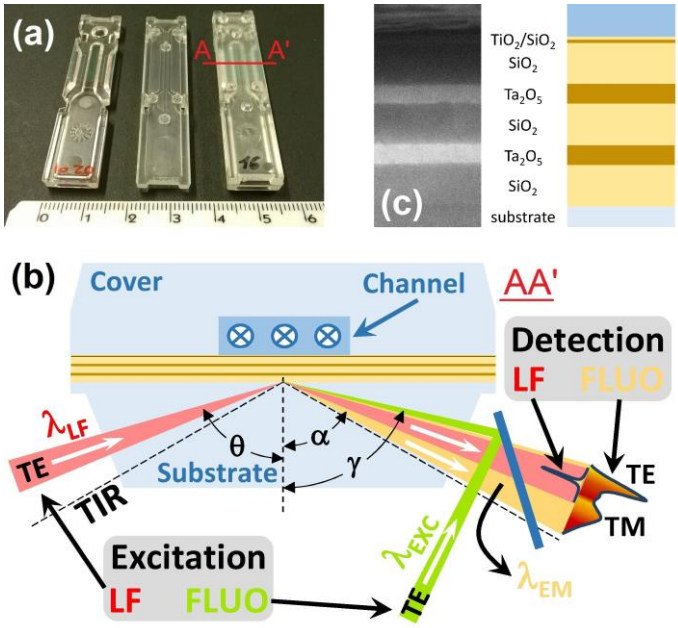

Figure 1 (color online) (a) Photographs of (left) organic substrate with the 1DPC deposited onto the surface, (middle) two components flow cell cover, (right) assembled biochip. (b) Schematic of the chip cross-section. (c) FESEM image of the 1DPC cross section and 1DPC geometry.

3. OPTICAL READOUT APPARATUS

The 1DPC biochips, including microfluidics, were mounted on an optical read out apparatus, whose operation principle is sketched in Figure 1b. During an assay the biochip was kept at constant temperature (T_M = 30°C).

In the label-free (LF) mode, a TE polarized laser beam at λ_{LF} was focused at the surface of the biochip through the coupling prism in a wide range of θ (FWHM above 4 deg) and above the TIR angle. BSW excitation at the biochip's surface causes dissipation of the incident intensity and the appearance of a resonant dip at θ_{BSW} in the angular spectrum of the reflected beam. θ_{BSW} depends on the dispersion of the BSW at λ_{LF} [1]. The role of the top TiO_2 layer was to tune absorption and scattering, therefore optimizing the contrast of the dip [28]. In a LF assay, binding of biomolecules perturbs the surface refractive index and θ_{BSW}. Tracking θ_{BSW} permits monitoring the binding kinetics and evaluating the surface density of bound biomolecules [29].

In the fluorescence (FLUO) mode, the biochip was excited at an angle γ above TIR by a TE polarized and slightly focused ($\Delta\gamma_{exc}$ = 0.64 deg) laser beam at λ_{EXC} = 635 nm. In a FLUO assay, any fluorescently labelled protein that is captured at the biochip surface can be excited and emit. As fluorescent labels we selected either Dylight 650 or Alexa Fluor 647 [30], since λ_{EXC} and λ_{LF} match their absorption and emission peaks, respectively [1]. γ was tuned to excite the BSW at λ_{EXC} with a resonantly enhanced intensity at the 1DPC surface, giving rise to an increased fluorescence excitation rate [8]. The emission at $\lambda_{EM} > \lambda_{EXC}$ was channelled to both the TE and TM polarized BSW modes, given their large LDOS [11], and then radiated through the substrate. Each spectral component at λ_{EM} was emitted at a different angle $\alpha < \gamma$ due to the spectroscopic role played by the BSW dispersion, which is polarization dependent [1].

In Figure 2 we show the layout of the optical apparatus that implemented the functions sketched in Figure 1b.

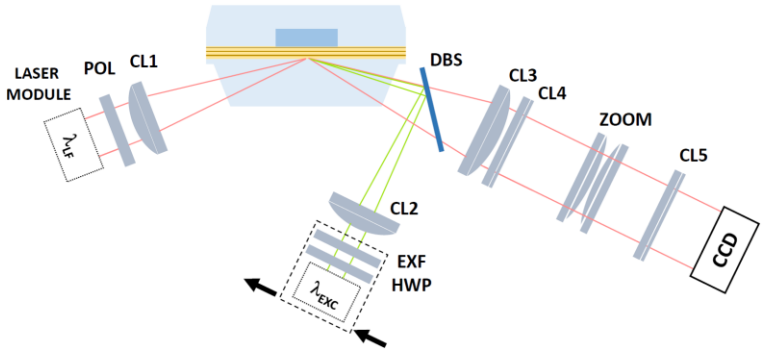

Figure 2 (color online) Sketch of the optical readout apparatus.

In the LF excitation arm, a laser module included a TE-polarized laser diode at λ_{LF}, the beam shaping and collimating optics and a rotating scatterer that destroyed the spatial coherence to avoid speckles upon detection. The polarization was refined by a polarizer (POL) aligned to the TE direction and the beam was focused onto the biochip by a cylindrical lens (CL1). In the detection arm, the illuminated line was imaged by a cylindrical Fourier lens (CL3) along the long axis of a monochrome CCD camera (Apogee Ascent,

Sony ICX814 chip). The cylindrical optics permitted to illuminate a line at the surface of the biochip and to access in a parallel manner to any spot along such a line. The angular field of view was 2.7 deg, as determined by CL3 and the width of the CCD array (12.50 mm, 3388 pixel). The spots along the illumination line were imaged along the short axis of the CCD array (10.00 mm, 2712 pixel) by a telecentric optical system, constituted by two cylindrical lenses, CL4 and CL5. Such a lateral optics cold image a 6 mm wide region along the illumination line with a lateral resolution below 100 μm, therefore allowing for the simultaneous analysis of 60 spots.

In the FLUO excitation arm, a laser module included a TE-polarized laser diode at λ_{EXC}, a half wave plate (HWP) that was used to adjust the polarization direction and an excitation filter (EXF, Chroma ZET 635/20). A cylindrical lens CL2 focused the beam into a line at the chip surface in the same position of the LF case. The laser module could be translated by means of a motorized stage, thus tuning the average incidence angle γ. The excitation beam was directed towards the biochip in an epifluorescence configuration by means of a dichroic beam splitter (DBS, Chroma ZT 640 RDC), which reflected the excitation beam and transmitted the fluorescence emission. Since λ_{EM} was around λ_{LF} we could make use of the same collection optics used for the LF case. However, an extra zoom lens (ZOOM) was inserted in the path in order to increase the angular field of view to 8 deg. Moreover, an emission filter (EMF, Chroma 655 LP ET) was placed along the path to cut stray light from the excitation beam.

4. BIOCHEMICAL FUNCTIONALIZATION

The 1DPC biochips were chemically and biochemically modified making use of different procedures. We prepared sets of biochip types, from B1 to B6 as listed in Table 1, with the aim to obtain a wide spectrum of the binding strengths of dye-labelled proteins to the 1DPC surface. Such chips were used in experiments with labelled neutravidin proteins aimed at studying PB and rotational diffusion under different conditions. Some of the type B6 biochips were functionalized with specific antibodies to give the B7 type and used in cancer biomarkers detection assays.

Biochemical reagents

Sulfuric acid (95–98%), hydrogen peroxide (30% in H_2O), (3-Aminopropyl) triethoxysilane (APTES, 99%), ethanol (99.8%), glutaraldehyde solution (GAH, grade I, 50% in H_2O), sodium bicarbonate (99.7%), sodium cyanoborohydride ($NaCNBH_3$, 95%), bovine serum albumin (BSA, 98%), and Dulbecco's Phosphate Buffered Saline 10X, (D-PBS 10X, 100 mM) were purchased from Sigma-Aldrich and used as received. For the experiments with biochip types B1 to B6, we used as a labelled protein NeutrAvidin

Protein, DyLight 650 (NAv650) and, only for the B5 type, a biotin-based crosslinker (EZ-Link NHS-Biotin), both from Thermo Fisher Scientific. For the cancer biomarker detection assay, biochip type B7, we labelled the detection antibodies with Alexa Fluor 647 NHS Ester purchased from Thermo Fisher Scientific.

Table 1 Biochip types and their chemical termination. C is the concentration of the NAv650 solution injected in each assay, washing indicates whether the FLUO measurements were performed with the NAv650 solution in the fluidic channel or after washing with D-PBS 1X, k_BT/ζ and σI_{exc} are the parameters values fitted from Figure 7.

Biochip	Termination	C [μg/ml]	Washing	k_BT/ζ [10^{-3} s^{-1}]	σI_{exc} [10^{-3} s^{-1}]
B1	Bare	1	No	> 13.3	19.0
B2	Piranha	1	Yes	0.54	34.8
B3	BSA	10	No	> 4.5	16.1
B4	APTES	1	Yes	1.5	8.0
B5	Biotin	0.5	Yes	0.79	6.0
B6	GAH	0.2	Yes	1.7	25.8

Surface modification of the 1DPC biochips

The first step of the chemical surface functionalization for all biochip types, except for the B1 type (bare), was a piranha treatment [31] to increase the hydroxyl groups density and remove contaminants, leading to the B2 biochips.

A subset of B2 biochips was de-activated allowing to react with a 1 mg/mL BSA solution in D-PBS 1X (blocking solution), leading to the B3 biochips. A second subset of B2 biochips was immersed in 2% (3-aminopropyl) triethoxysilane (APTES) in a mixture of ethanol/water (95/5 v/v) for 1h at ambient temperature, followed by sonication, washing in ethanol, and soft-baking on a hot plate at 110 °C for 1 h, leading to the B4 biochip.

A subset of B4 biochips was biotinylated making use of EZ-Link NHS-Biotin to exploit the high affinity of biotin for the labelled neutravidin. Biotinylization was followed by a de-activation step in the blocking solution, leading to the B5 biochips. A second subset of B4 biochips was immersed in 2% GAH in bicarbonate buffer for 1h at ambient temperature adding $NaCNBH_3$, followed by sonication and washing in deionized water, leading to the B6 biochips.

Finally, a subset of B6 biochips was tailored with monoclonal antibodies for specific antigen recognition,

leading to the B7 biochip. Details on the cancer biomarker protocol and specific antibodies are in the next paragraph.

Such different chemical terminations can hinder the rotation of bound proteins to a larger/smaller extent, which however does not necessarily correspond to a larger/smaller protein capture efficiency and mass surface coverage.

Protocols for the cancer biomarker detection assay

As an application of 1DPC biochips to cancer biomarkers detection, we addressed the tyrosine kinase receptor (ERBB2) involved in a variety of cell proliferation, growth and differentiation pathways. In particular, ERBB2 gene amplification/overexpression occurs in approximately 20–30% of breast cancers [32]. An ERBB2 positive cell line, BT474, was selected as a source of ERBB2 cancer biomarkers [33]. Cells were counted by Trypan Blue exclusion and lysed under non-denaturing conditions with an ice-cold lysis buffer supplemented with 1mM phenyl-methane-sulfonyl fluoride. Yields of whole cell lysates were assessed by the bicinchoninic acid (BCA) assay.

Biochips of the B7 type were prepared by immobilizing in three regions of the surface along the illumination line, a specific capture mAb (cAnti-ERBB2), a non specific mAb (L31) and BSA, which was the negative reference. Finally, the whole biochips' surface was de-activated by immersing in the blocking solution overnight at +4°C.

The specific capture mAb (cAnti-ERBB2) was the custom antibody W6/300G9 [34]. The non-specific mAb used for internal referencing, was the irrelevant specificity L31 antibody, which binds human Major Histocompatibility Complex class I (MHC I) molecules [35]. For FLUO detection, we used as a detection mAb the proprietary antibody W6/800E6, which was conjugated to the NHS ester of Alexa Fluor 647 to provide a fluorescent detection mAb (dAnti-ERBB2). All mAbs were dissolved in D-PBS 1X. cAnti-ERBB2 and dAnti-ERBB2 were developed to target distinct epitopes of the ERBB2 ectodomain [34,35] for capture and detection, respectively.

5. PLATFORM OPERATION

The inset in Figure 3a shows the CCD image acquired in the LF mode for a bare biochip (B1 type) operating in water. The BSW excitation at λ_{LF} appeared as a dark vertical line. The superimposed curve is the angular reflectance averaged between the two dark dashed lines, corresponding to a 0.56 mm wide spot of the illuminated line. θ_{BSW} slightly changed along the line, due to the 1DPC inhomogeneity. The sensitivity with

respect to changes of n_{sol} was measured in experiments with calibrated refractive index solutions and was $S_V = \partial\theta_{BSW} / \partial n_{sol} = 34.1$ deg / RIU, where RIU is refractive index units.

Figure 3a shows sensorgrams recorded when 220 µl of a 1 µg/ml solution of NAv650 in D-PBS 1X were continuously injected in a biochip at 1.35 µl/s flowrate. The relative shift $\Delta\theta_{BSW}(t) = \theta_{BSW}(t) - \theta_{BSW}(0)$ was continuously tracked in order to monitor in real-time the NAv650 capture at the surface. The curves were recorded in three different assays carried out with biochips of the B1, B2, and B4 type. The sensorgrams are the average of the curves recorded in ten different 0.11 mm wide spots. Clearly, the biochip prepared with APTES (B5) captured much more NAv650 than the piranha treated (B2) and bare (B1) biochips. At the end of the NAv650 incubation, at t = 15 min, the biochips were washed by injecting D-PBS 1X. The residual shifts $\Delta\theta_{RES}$ were 1.2 mdeg, 9 mdeg and 112 mdeg, for the B1, B2 and B4 biochips respectively. From the $\Delta\theta_{RES}$ values we calculated the surface density of bound NAv650 by means of the De Fejter's formula [36].Since each NAv650 bears two Dylight 650 molecules in average [30], the resulting surface density of fluorescent molecules was 2.0×10^{10} cm^{-2}, 1.6×10^{11} cm^{-2}, 1.9×10^{12} cm^{-2}, respectively for the B1, B2 and B4 biochips.

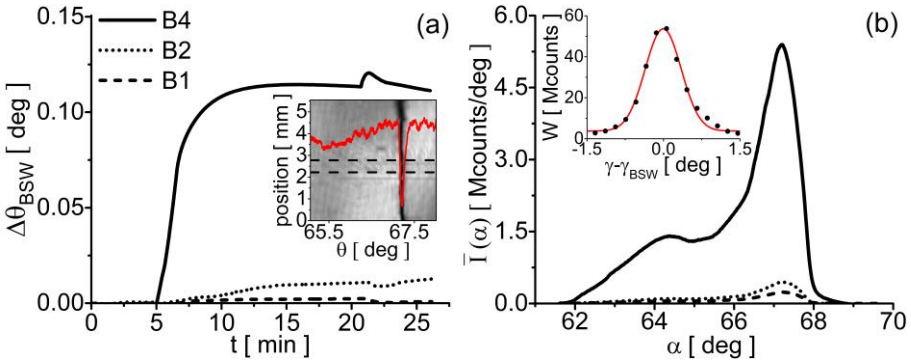

Figure 3 (color online) (a) LF sensorgrams recorded when NAv650 in D-PBS was continuously injected in three biochips types: (dashed) B1, (dotted) B2, (solid) B4. Inset: CCD image acquired in the LF mode at λ_{LF} = 670 nm. (b) Background subtracted FLUO measurements at the end of the LF assay for each biochip (same curve coding). Inset: W vs γ for the B4 type case.

Figure 3b shows the CW angular fluorescence emission spectra recorded by the CCD camera under TE polarized excitation at λ_{EXC} and at resonant angle γ. The three curves were obtained for the same biochips, of the B1, B2 and B4 type, used in the LF assays shown in Figure 3a. For each biochip, the curves are the difference between the spectra recorded in D-PBS after and before incubating the NAv650 solution and are averaged over the same rows of the CCD image used for the LF case. The experimental data are in good agreement with the predictions based on our theoretical models, showing two TM and TE angularly dispersed bands. [1] The inset of Figure 3b shows the measurement of the fluorescence power $W = \int I(\alpha)d\alpha$ as a function of the detuning of the excitation angle from the resonant excitation condition

$\gamma - \gamma_{BSW}$, for the B4 type case, indicating that resonant excitation and emission were reached when γ matched the γ_{BSW} resonant angle at λ_{EXC}. The quality factor of the fluorescence excitation curve shown in the inset was $Q_{FLUO} = \gamma_{BSW}/\Delta\gamma_{FWHM} = 11.1$. All curves reported in figures showing $I(\alpha)$ distributions that will follow were obtained at γ_{BSW}.

The results of the LF and FLUO measurements shown in Figure 3 are in a good agreement. As an example, the ratio of the $\Delta\theta_{RES}$ values found in the LF mode for the B4 and B2 biochips is 12.4, which corresponds quite well to the ratio of the P values found in the FLUO mode that was 13.2.

6. EFFECT OF THE ANISOTROPIC PHOTOBLEACHING

We report here on real-time experiments on anisotropic PB and orientational diffusion of proteins bound at the 1DPC surface to be compared to our theoretical models [1]. Since we refer to some specific observables, we briefly recall here the Smoluchowsky-Einstein equation that governs rotational diffusion of an ensemble of rod-like molecules in a host medium and taking into account PB:

$$\frac{\partial f(\theta,\varphi,t)}{\partial t} = \frac{k_B T}{\zeta}\frac{1}{sin\theta}\frac{\partial}{\partial\theta}\left(sin\theta\,\frac{\partial f(\theta,\varphi,t)}{\partial\theta}\right) + \frac{k_B T}{\zeta}\frac{1}{sin^2\theta}\frac{\partial^2 f(\theta,\varphi,t)}{\partial\varphi^2} - \sigma I_{exc} f(\theta,\varphi,t) sin^2\theta sin^2\varphi \qquad (1)$$

where $f(\theta,\varphi,t)$ is the orientational distribution function, $k_B T$ is the thermal energy and ζ is a friction coefficient between a molecule and the host medium [38]. $\theta = 0$ is the normal to the 1DPC and molecules can undergo PB with cross section σ by a TE polarized ($\theta = \varphi = \pi/2$) illumination field with intensity I_{exc}. Full details on the solution of the Eq.(1) are given elsewhere [1]. The two observables that we shall deal with experimentally are σI_{exc} and $k_B T/\zeta$.

Figure 4a shows a sketch of the 1DPC surface with labelled proteins bound to different extents. The dye probes orientation wobbles in a cone [39] (red) while the overall orientation of the probe-protein complex can change due to orientational diffusion (grey). Such a condition is generally referred to as cone-in-a-cone model [40]. Here we assume that wobbling is very fast [18] and that dye probes are aligned along the cone axis. Contrarily, we assume that the depolarization of the complex is slow, based on our experimental observation that evidence very long time scale effects during the experiments discussed below.

For the moment, as an example, we limit the description of our experiments to the case of a biochip of the B6 type. The biochip was mounted on the readout system, the fluidic channel was filled with D-PBS 1X and the fluorescence background was acquired. Then, 160 µl of a 200 ng/ml NAv650 solution in D-PBS 1X were injected into the fluidic channel and 10 µl of the solution were recirculated back and forth for

15 min (20 times) during incubation and binding of NAv650. At the end we washed with D-PBS 1X and kept the biochip in dark.

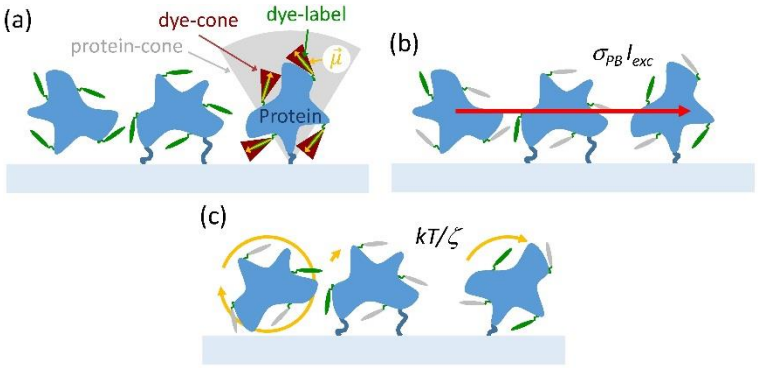

Figure 4 (color online) (a) 1DPC surface with bound dye-labelled proteins; (b) Selective PB by means of a TE polarized field; (c) Depolarization of proteins.

At t=0 we started exciting under CW conditions the biochip in the FLUO mode at λ_{EXC}, at resonant γ_{BSW} and with TE polarization. Figure 5 shows the background subtracted angular fluorescence $I(\alpha)$ that was continuously acquired at fixed time intervals. The curves were averaged over 0.34 mm wide spots. During the CW illumination $I(\alpha)$ decreased along time, due to the overall decrease of the number of active emitters that were undergoing PB. However, a more detailed analysis of the curves shows that the relative peak amplitudes of the TE and TM bands, I_{TE}^{peak} and I_{TM}^{peak} changed along time, indicating that not only the number of emitters but also that their orientational distribution was changing. As sketched in Figure 4b, the excitation beam photoselects those dye molecules with a component of the transition dipole moment along the TE direction [3], leading to an anisotropic PB. Due to the reduced orientational mobility of the NAv650 complexes, which are bound at the biochip surface, anisotropic PB prevails over depolarization, whose effect is depicted in Figure 4c, and $f(\theta, \varphi, t)$ is modified. Thus, since coupling to the TE and TM BSW depends on the emitters' orientation, the relative intensities of the bands change along time. The curves in Figure 5 are in very good agreement with the results of our theoretical model, involving the full calculation of the polarization dependent emission rates. [1]

Figure 6a shows a semi-log plot of the time dependence of I_{TE}^{peak} and I_{TM}^{peak} during the experiment, both showing a multiple exponential decay. Due to the resonant CW excitation and field enhancement at γ_{BSW}, the PB process is very fast. For the fluorescence excitation laser power used in the experiments (4mW), I_{TE}^{peak} decreased by a factor 10 in 0.38 min and by a factor 100 in 3 min. This result sets a serious obstacle to the quantitative evaluation of the absolute intensity in cancer biomarker detection assays based on photonic crystal enhanced fluorescence, especially when low concentrations are targeted and long

integration time intervals are involved. For longer illumination times the curves continue decaying with longer time constants.

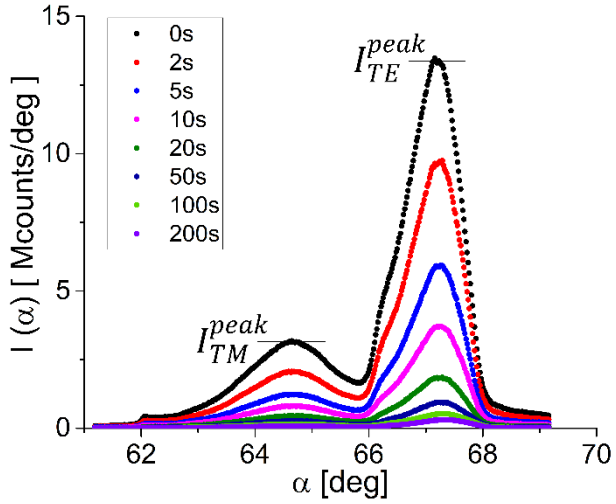

Figure 5 (color online) $I(\alpha)$ recorded at fixed time intervals during CW fluorescence excitation for NAv650 bound at the surface of B6 biochips.

In Figure 6b we plot the temporal dependency of the ratio $R = I_{TE}^{peak}/I_{TM}^{peak}$, showing that indeed it was not constant during the measurement. The ratio was about $R(0) = 6.1$ at t =0, as it is expected for an isotropic orientational distribution of the emitters under TE excitation [1]. In a first phase (light grey background), $R(t)$ decreased and reached the value 3.5 after about 7 min, when I_{TE}^{peak} and I_{TM}^{peak} had decreased by a factor 165. The inset of Figure 6b shows the detail of the experimentally measured $R(t)$during such a first phase together with the result of our theoretical model (red solid line). The experiment is consistent with the theoretical model, when setting for the PB rate and the rotational diffusion coefficient the values $\sigma I_{exc} = 0.0258\ s^{-1}$ and $k_B T/\zeta = 0.0017\ s^{-1}$, respectively [1].

In a second phase (white background), $R(t)$ increased again. Such an increase was due to the fact that the collected fluorescence was originating both from proteins bound at the biochip surface and from residual proteins in solution and in proximity to the biochip surface. Such latter proteins could freely rotate and were therefore characterized by an isotropic orientation distribution with a constant $R(0) = 6.1$. During the first phase, the contribution of the bound proteins dominates. However, during the second phase, the distribution of the dye emitters conjugated to the proteins bound at the surface was more and more depleted along the illumination direction and the residual fluorescence originated from those in solution, therefore driving $R(t)$ back towards $R(0)$.

Figure 6a (dark grey background) also shows that, when the fluorescence excitation beam was shut (t = 42.3 min) and then opened again (t = 53.9 min), there was a recovery of the fluorescence intensity and

again a steep decay. Such result indicates that when the excitation beam was turned off the $f(\theta, \varphi, t)$ of the surface bound emitters relaxed to the isotropic distribution, leading to a partial recovery of R(t) towards the isotropic value.

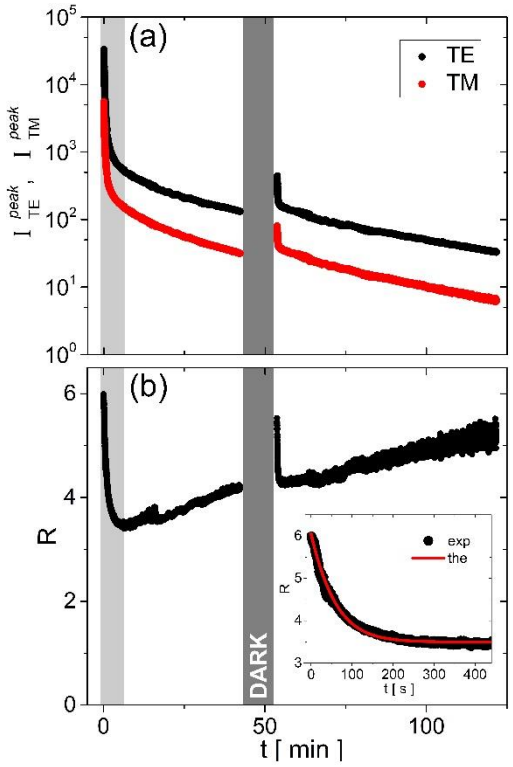

Figure 6 (color online) (a) I_{TE}^{peak} and I_{TM}^{peak} and (b) $R(t)$ measured during CW fluorescence excitation for NAv650 bound at the surface of B6 biochips. The dark grey band marks the interval when the FLUO excitation laser was shut. The inset is a detail of the light grey shaded region.

7. DISCUSSION

The results shown in Figure 6 and their agreement with our theoretical model indicate that anisotropic PB strongly affects fluorescence of organic molecules in proximity of the surface of a 1DPC biosensor sustaining BSW and in general of resonant PC structures.

On one hand, as widely accepted in fluorescence microscopy [3], labels with as minimum as possible PB cross section σ should be used when designing reliable assay formats for biomarkers detection with PC biochips. Core-shell semiconductor quantum dots have been proposed as a solution [3]. However, single-molecule spectroscopy reveals that also quantum dots can readily photobleach and photoblink [41], casting doubts on their application in biosensing when very small biomarkers' concentrations are targeted [42]. Therefore, whatever the labeling, PB and its strong polarization dependency must be anyhow mastered when dealing with highly resonant PC biosensors.

On the other hand, BSW mediated anisotropic PB can be exploited to probe rotational diffusion of any protein labelled with fluorescent emitters. Due to their surface localization, BSW permit to probe only those proteins bound at the interface. Moreover, the polarization dependent spectroscopic role played by the 1DPC permits to analyze simultaneously two polarizations within a relatively simple optical layout. Thus, when properly mastered, anisotropic PB becomes an opportunity rather than a problem.

In the following we report two examples in which PB is either exploited for the investigation of protein rotation or compensated in cancer biomarkers' detection assays.

Rotational diffusion of proteins bound to a surface with different strengths

Figure 7 shows the results obtained for B1, B2 and B3 biochips during the first phase of the experiments, together with the B6 biochip result already shown in Figure 6. For all experiments we used the same protocol. In the B1 and B3 cases, $I(\alpha)$ was acquired with the microfluidic channel filled with the NAv650 solution, with the aim to probe the emission of freely rotating proteins in solution. All other biochips were washed thoroughly with D-PBS 1X after NAv650 incubation, in order to remove proteins in solution.

Figure 7 shows that $R(t)$ can be driven very far from the isotropic value $R(0)$ for proteins bound at the biochip surface (B2 and B6), whereas it keeps close to $R(0)$ for freely rotating proteins (B1 and B3).

The curves in Figure 7 were fitted to our theoretical model [1] with only σI_{exc} and $k_B T_M/\zeta$ as free parameters. In Table I we list the fitted values.

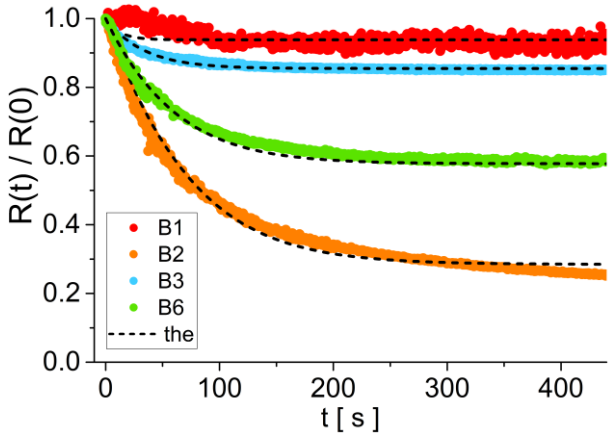

Figure 7 (color online) $R(t)/R(0)$ measured in experiments with four biochips of different types. The dashed curves are theoretical fits.

The σI_{exc} values are all of the same order of magnitude. The variations, despite the results were obtained for the same excitation power, are possibly due to different local values I_{exc} at the biochips' surface, keeping with the fact that the BSW resonance width and the field enhancement factor are influenced by

surface loading. As an example, the biochip B3 shows the lowest σI_{exc} since the BSA layer keeps the emitters at a larger distance from the 1DPC surface where I_{exc} is smaller [1].

The $k_B T_M/\zeta$ values span over a wider relative range, confirming that indeed rotational diffusion is strongly influenced by the reactivity of the biochips' surface. For the B1 and B3 biochips, probably the signal was due to both a volume and a surface contribution, the latter due to proteins that bound nonspecifically to either the bare or the BSA de-activated surface. After an initial fast decay due to PB of the surface emitters, the $R(t)/R(0)$ curves keep constant, as it is expected for a constant population of freely rotating emitters. Therefore the fitted $k_B T_M/\zeta$ for the B1 and B3 biochips are likely to be underestimated.

Table I indicates that a piranha treated surface (B2) hindered rotational diffusion more than any other case. Proteins were captured less efficiently, as shown by Figure 3, but they were bound more tightly, probably by multiple bonds. The values for the GAH biochip (B6) show a roughly three times larger rotational diffusion coefficient, while the bare (B1) and BSA (B3) biochips keep well with the case of freely rotating emitters.

Further experiments (not shown), carried out with either B4 or B5 biochips, gave the $k_B T_M/\zeta$ values listed in Table I, which are between the B2 and the B6 cases. The biotin surface (B5) hindered rotation more than the APTES one (B4), which was similar to the GAH one (B6). However, the large deviations of the σI_{exc} values suggest that the experiments for the B4 and B5 biochips should be refined.

Table I shows that $k_B T_M/\zeta$ increases when increasing the number of intermediates between the surface and the proteins, from biochip B2 to B4 and to B6. The only exception is the B5 type, which shows to hinder rotation more than B4 and B6. However, latter case can be explained by the extreme affinity of biotin for NAv650, which possibly provides multiple binding of NAv650 to the biochip surface.

The values for $k_B T_M/\zeta$ reported in Table 1 are much smaller than those reported in literature for proteins in solution ($2 \times 10^7 s^{-1} > k_B T_M/\zeta > 4 \times 10^6 s^{-1}$) [3] and for proteins in cell membranes (eosin, $k_B T_M/\zeta \sim 10^3 s^{-1}$) [15], as expected since NAv650 was bound at the biochip surface and behaved as a hindered rotor. We observe that, under such conditions, standard fluorescence anisotropy time-resolved techniques [3] do not provide a characterization of rotational diffusion, since the diffusion time is much longer than the fluorescence lifetime. In those cases, such a long living term is modeled by a residual and constant anisotropy value.

Cancer biomarkers' detection assays

Figure 8a shows the LF sensorgrams recorded during an assay carried out with a B7 biochip. θ_{BSW} was

recorded in the three biochip's regions where c-Anti-ERBB2 (positive), L31 (negative) and BSA (reference) were immobilized. The curves are the average over 4 adjacent spots, each 45 μm wide, except for the BSA region, where 3 spots were averaged. At t = 0 min, the biochip was filled with the D-PBS 1X solution. At t = 7 min, 220 μL of a BT-474 cell lysate at a whole protein concentration 0.5 mg/ml were injected at a flow rate of 1.35 μL/s. Once the injection was completed, 20 μL were re-circulated back and forth 20 times. At t = 17 min, the biochip was rinsed with D-PBS 1X. At t = 22 min, we injected a solution of D-PBS 2.5X and then rinsed at t = 26 min with D-PBS 1X; the angular shift recorded at the buffer change was used to calibrate for small variations of the 1DPC LF sensitivity along the biochip surface. At t = 32 min, the platform was switched to the FLUO mode to collect the fluorescence background when exciting at γ_{BSW}. Then the platform was switched back to the LF mode at t = 35 min. At t = 39 min, 220 μL of dAnti-ERBB2 in D-PBS 1X at a concentration of 10 μg/mL were injected at a flow rate of 1.35 μL/s and re-circulated with the same protocol described above.

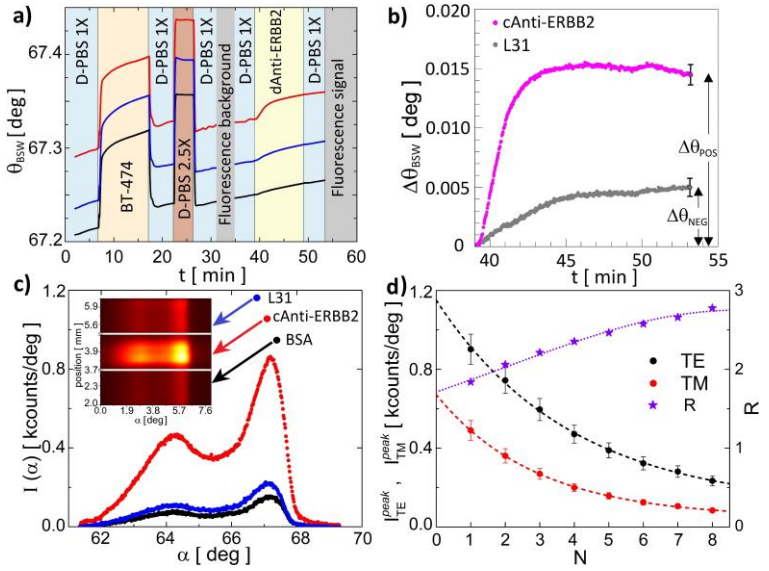

Figure 8 (color online) Assay for ERBB2 with a B7 biochip. (a) LF sensorgrams in the regions: (black) BSA, (blue) L31, (red) cAnti-ERBB2. (b) Differential LF signals during the dAnti-ERBB2 incubation phase: (grey) L31-BSA, (violet) cAnti-ERBB2-BSA. (c) $I(\alpha)$ in the regions: (black) BSA, (blue) L31, (red) cAnti-ERBB2. Inset: CCD image (d) I_{TE}^{peak}, I_{TM}^{peak} and R vs N for 8 repeated FLUO measurements.

The time t = 49 min marks the end of the LF assay, when the biochip was washed with D-PBS 1X to remove the excess dAnti-ERBB2. In Figure 8b the differential signals, obtained by subtracting to both the dAnti-ERBB2 and L31 curves the BSA one, are presented. A residual angular label-free shift $\Delta\theta_{RES}$ could be measured in both the positive and negative regions, as listed in Table 2.

The time t = 49 min also marks the beginning of the FLUO assay, in which the background subtracted $I(\alpha)$ at γ_{BSW} was collected repetitively for 8 times. Figure 8c shows the $I(\alpha)$ curves averaged over the same spots used in the LF case. The $I(\alpha)$ curves were extracted from the CCD image shown in the inset of Figure 8c, showing that the cAnti-ERBB2 region is clearly distinguishable and confirming that the ERBB2 biomarker was efficiently captured by the cAnti-ERBB2 region, compared to the BSA and L31 regions.

The effect of PB is clearly visible when comparing the $I_N(\alpha)$ of the 8 successive fluorescence measurements. Figure 8d shows the fitted values for I_{TE}^{peak}, I_{TM}^{peak} and their ratio R as a function of the number of measurement N, for the cAnti-ERBB2 region. Similar data were obtained for the L31 and BSA regions. The dependence could be fitted with the single exponential behavior predicted by the theoretical model [1] for short illumination times (that observed in the grey region of Figure 6a). The fits were used to extrapolate $I_{TE}^{peak}$and I_{TM}^{peak} to N=0 and to evaluate the PB-free spectra $I_{N=0}(\alpha)$. Finally, the $I_{N=0}(\alpha)$ were integrated over α to get the fluorescence power W, which was corrected by dividing by the square of Q_{FLUO} (Figure 3b) averaged over each region. The quadratic normalization originates from the assumption that, for the small deviations observed for Q_{FLUO} (±20%), both the coupling efficiency of the fluorescence excitation beam to the TE BSW [37] and the spontaneous fluorescence rate of the emitters when coupled to the BSW resonant modes [43] scale linearly with Q_{FLUO}.

Table 2 – Results of the combined LF and FLUO ERBB2 assay

Mode	Signal	cAnti-ERBB2 – BSA	L31 – BSA	Ratio
LF	$\Delta\theta_{RES}$ [mdeg]	15.7 ± 2.1 (13%)	4.7 ± 1.5 (32%)	3.4 ± 1.6 (47%)
FLUO	ΔW [MCounts]	2.96 ± 0.17 (6%)	0.64 ± 0.02 (3%)	4.6 ± 0.4 (9%)

In Table 2, we list the differential power ΔW, calculated either as W(cAnti-ERBB2)-W(BSA) or as W(L31)-W(BSA) and their ratio. The result shows that both the LF and FLUO assays distinguish the positive and negative regions and that, within the errors, they give the same result for the ratio and are therefore calibrated. Moreover Table 2 confirms that the coefficient of variation of the FLUO assay is lower that the LF case, providing a smaller limit of detection, as already reported experimentally elsewhere [31].

Figure 8d also shows that during illumination R_N grows towards a plateau in the range of that observed in the first part of Figure 6. Such a behavior is consistent with our theoretical model [1] for emitters that are preferentially aligned normal to the 1DPC at the beginning. Such a result is possibly due to the fact that during the LF assay, despite that the illumination power is very low, that the focusing is weak and that λ_{LF} is in the low absorption region for the dye labels, PB took place and modified $f(\theta, \varphi, t)$ by burning a hole along the TE direction. The result suggests that the LF signal during the dAnti-ERBB2 incubation should be sampled at low frequency rather than measured under CW illumination.

8. CONCLUSIONS

We experimentally characterized the anisotropic PB effects taking place during the operation of 1DPC biosensors sustaining BSW. The experimental results are in very good agreement with the description provided by our theoretical model [1]. We demonstrated experimentally that the LF and FLUO results of a cancer biomarkers' detection assay agree when PB is correctly analysed and compensated for. Finally, we showed that BSW coupled fluorescence, in association with the anisotropic PB and the strong localization of the BSW at the 1DPC surface, permit to probe selectively the rotational diffusion kinetics of proteins bound at the 1DPC surface with high spatial resolution and for different binding strengths.

ACKNOWLEDGEMENTS

We thank P. Giacomini and M. Allegretti (IFO/IRE) for the lysates and the mAb used in the ERBB2 assays, F. Mura (SAPIENZA-CNIS) for the FESEM image and A. Occhicone for fruitful discussions. This work was funded by the European Commission (BILOBA, 318035) and by the Regione Lazio (TURNOFF, 85-2017-14945).

REFERENCES

1. F. Michelotti and E. Sepe, "Anisotropic Fluorescence Emission and Photobleaching of Fluorophores in Proximity of One Dimensional Photonic Crystals sustaining Bloch Surface Waves. I. Theory," Optica (n.d.).
2. A. P. Demchenko, *Introduction to Fluorescence Sensing*, 2nd ed. (Springer Nature Switzerland AG, 2009).
3. J. R. Lakowicz, *Principles of Fluorescence Spectroscopy*, Third Edit (Springer US, 2006).
4. P. Yeh, A. Yariv, and C.-S. Hong, "Electromagnetic propagation in periodic stratified media I General theory*," J. Opt. Soc. Am. **67**, 423–438 (1977).

5. K. Toma, M. Vala, P. Adam, J. Homola, W. Knoll, and J. Dostálek, "Compact surface plasmon-enhanced fluorescence biochip," Opt. Express **21**, 10121 (2013).
6. A. Sinibaldi, A. Fieramosca, R. Rizzo, A. Anopchenko, N. Danz, P. Munzert, C. Magistris, C. Barolo, and F. Michelotti, "Combining label-free and fluorescence operation of Bloch surface wave optical sensors," Opt. Lett. **39**, 2947–2950 (2014).
7. R. Badugu, K. Nowaczyk, E. Descrovi, and J. R. Lakowicz, "Radiative decay engineering 6: Fluorescence on one-dimensional photonic crystals," Anal. Biochem. **442**, 83–96 (2013).
8. R. Rizzo, M. Alvaro, N. Danz, L. Napione, E. Descrovi, S. Schmieder, A. Sinibaldi, R. Chandrawati, S. Rana, P. Munzert, T. Schubert, E. Maillart, A. Anopchenko, P. Rivolo, A. Mascioletti, F. Sonntag, M. M. Stevens, F. Bussolino, and F. Michelotti, "Bloch surface wave label-free and fluorescence platform for the detection of VEGF biomarker in biological matrices," Sensors Actuators, B Chem. **255**, 2143–2150 (2018).
9. V. Chaudhery, M. Lu, C. S. Huang, S. George, and B. T. Cunningham, "Photobleaching on Photonic Crystal Enhanced Fluorescence Surfaces," J. Fluoresc. **21**, 707–714 (2011).
10. K. Toma, E. Descrovi, M. Toma, M. Ballarini, P. Mandracci, F. Giorgis, A. Mateescu, U. Jonas, W. Knoll, and J. Dostálek, "Bloch surface wave-enhanced fluorescence biosensor," Biosens. Bioelectron. **43**, 108–114 (2013).
11. S. D. Choudhury, R. Badugu, and J. R. Lakowicz, "Directing Fluorescence with Plasmonic and Photonic Structures," Accounts Chem. Res. **48**, 2171–2180 (2015).
12. F. Perrin, "Polarisation de la lumière de fluorescence . Vie moyenne des molécules dans l ' etat excité," **7**, 390–401 (1926).
13. A. Sinibaldi, A. Fieramosca, N. Danz, P. Munzert, A. Occhicone, C. Barolo, and F. Michelotti, "Effects of Reabsorption due to Surface Concentration in Highly Resonant Photonic Crystal Fluorescence Biosensors," J. Phys. Chem. C **122**, 26281–26287 (2018).
14. T. Ha, T. Enderle, and D. S. Chemla, "Single Molecule Dynamics Studied by Polarization Modulation," Phys. Rev. Lett. **77**, 3979–3982 (1996).
15. R. J. Cherry, "Measurement of protein rotational diffusion in membranes by flash photolysis," Methods Enzymol. **LIV**, 47–61 (1978).
16. E. Betzig and R. J. Chichester, "Single Molecules Observed by Near-Field Scanning Optical Microscopy EJ2," Science (80-.). **262**, 1422–1425 (1993).
17. T. Ha, J. Glass, T. Enderle, D. S. Chemla, and S. Weiss, "Hindered Rotational Diffusion and Rotational Jumps of Single Molecules," Phys. Rev. Lett. **80**, 2093–2096 (1998).
18. C. Augusto, V. Cruz, H. Ahmed, A. Kress, N. Bertaux, S. Monneret, M. Mavrakis, J. Savatier,

and S. Brasselet, "Quantitative nanoscale imaging of orientational order in biological filaments by polarized superresolution microscopy," PNAS **113**, E820–E828 (2016).

19. M. P. Backlund, M. D. Lew, A. S. Backer, S. J. Sahl, G. Grover, A. Agrawal, R. Piestun, and W. E. Moerner, "Simultaneous , accurate measurement of the 3D position and orientation of single molecules," PNAS **109**, 19087–19092 (2012).
20. A. Uvarov and S. Fritzsche, "Restricted Rotational Diffusion of Non-rigid Dumbbell-Type Macromolecules on Surfaces : Effects of the Bead-Bead and Bead-Surface Interaction," Progr Colloid Polym Sci **133**, 95–99 (2006).
21. M. M. G. Krishna, R. Das, N. Periasamy, and R. Nityananda, "Translational diffusion of fluorescent probes on a sphere : Monte Carlo simulations , theory , and fluorescence anisotropy experiment," J. Chem. Phys. **112**, 8502–8514 (2000).
22. P. Johnson and P. B. Garland, "Depolarization of fluorescence depletion. A microscopic method for measuring rotational diffusion of membrane proteins n the surface of a single cell," FEBS Lett. **132**, 252–256 (1981).
23. H. Raether, *Surface Plasmons* (Springer-Verlag, 1988).
24. N. Danz, A. Sinibaldi, P. Munzert, A. Anopchenko, E. Förster, S. Schmieder, R. Chandrawati, R. Rizzo, R. Heller, F. Sonntag, A. Mascioletti, S. Rana, T. Schubert, M. M. Stevens, and F. Michelotti, "Biosensing platform combining label-free and labelled analysis using Bloch surface waves," in *Proceedings of SPIE - The International Society for Optical Engineering* (2015), Vol. 9506.
25. "https://topas.com/," .
26. P. Munzert, N. Danz, A. Sinibaldi, and F. Michelotti, "Multilayer coatings for Bloch surface wave optical biosensors," Surf. Coat. Technol. **314**, 79–84 (2017).
27. F. Michelotti, A. Sinibaldi, P. Munzert, N. Danz, and E. Descrovi, "Probing losses of dielectric multilayers by means of Bloch surface waves," Opt. Lett. **38**, 616–618 (2013).
28. F. Michelotti, R. Rizzo, A. Sinibaldi, P. Munzert, C. Wächter, and N. Danz, "Design rules for combined label-free and fluorescence Bloch surface wave biosensors," Opt. Lett. **42**, (2017).
29. J. Homola, "Surface plasmon resonance sensors for detection of chemical and biological species," Chem. Rev. **108**, 462–93 (2008).
30. "https://www.thermofisher.com/," .
31. A. Sinibaldi, C. Sampaoli, N. Danz, P. Munzert, L. Sibilio, F. Sonntag, A. Occhicone, E. Falvo, E. Tremante, P. Giacomini, and F. Michelotti, "Detection of soluble ERBB2 in breast cancer cell lysates using a combined label-free/fluorescence platform based on Bloch surface waves," Biosens. Bioelectron. **92**, 125–130 (2017).

32. O. K. Mahfoud, T. Y. Rakovich, A. Prina-mello, D. Movia, F. Alves, and Y. Volkov, "Detection of ErbB2 : nanotechnological solutions for clinical diagnostics," RSC Adv. **4**, 3422–3442 (2014).
33. K. Subik, J.-F. Lee, L. Baxter, T. Strzepek, D. Costello, P. Crowley, L. Xing, M. Hung, T. Bonfiglio, D. G. Hicks, and P. Tang, "The Expression Patterns of ER , PR , HER2 , CK5 / 6 , EGFR , Ki-67 and AR by Immunohistochemical Analysis in Breast Cancer Cell Lines," Breast Cancer Basic Clin. Res. **4**, 35–41 (2010).
34. P. Giacomini, A. K. Ng, R. R. S. Kantor, P. G. Natali, and S. Ferrone, "Double Determinant Immunoassay to Measure a Human High-molecular-weight Melanoma-associated Antigen," Cancer Res. **43**, 3586–3590 (1983).
35. G. Digiesi, P. Giacomini, R. Fraioli, M. Mariani, M. R. Nicotra, O. Segatto, and P. G. Natali, "Production and Characterization of Murine mAbs to the Extracellular Domain of Human Neu Oncogene Product GP185HER2," Hybridoma **11**, 519–527 (1992).
36. A. Sinibaldi, A. Anopchenko, R. Rizzo, N. Danz, P. Munzert, P. Rivolo, F. Frascella, S. Ricciardi, and F. Michelotti, "Angularly resolved ellipsometric optical biosensing by means of Bloch surface waves," Anal. Bioanal. Chem. **407**, 3965–3974 (2015).
37. R. Ulrich, "Theory of the Prism-Film Coupler by Plane-Wave Analysis," J. Opt. Soc. Am. **60**, 1337 (1970).
38. M. W. Evans, J. Evans, W. T. Coffrey, and P. Grigolini, *Molecular Dynamics and Theory of Broad Band Spectroscopy* (Wiley, 1982).
39. K. J. Kinosita, S. Kawato, and A. Ikegami, "Polarization decay in membranes," Biophys. J. **20**, 289–305 (1977).
40. G. F. Schroeder, U. Alexiev, and H. Grubmueller, "Simulation of Fluorescence Anisotropy Experiments : Probing Protein Dynamics," Biophys. J. **89**, 3557–3770 (2005).
41. H. Cao, L. Huang, H. Qin, R. Meng, Y. Li, and X. Peng, "Design and Synthesis of Antiblinking and Antibleaching Quantum Dots in Multiple Colors via Wave Function Con fi nement," J Am. Chem. Soc. **138**, 15727–15735 (2016).
42. H. Qin, R. Meng, N. Wang, and X. Peng, "Photoluminescence Intermittency and Photo-Bleaching of Single Colloidal Quantum Dot," Adv. Mater. **29**, 1606923 (2017).
43. E. M. Purcell, "B10 - Spontaneous emission probabilities at radio frequencies," in *Proceedings of the American Physical Society - Physical Review* (1946), Vol. 69, p. 681.